LUNAR TOPOGRAPHIC MAPPING USING A NEW HIGH RESOLUTION MODE FOR THE GSSR RADAR

Scott Hensley, Eric Gurrola*, Leif Harcke*, Martin Slade*, Kevin Quirk*, Meera Srinivasan*, Clement Lee*, Sang-Ho Yun*, Joseph Jao*, Barbara Wilson*, Eric De Jong*, Nick Marechal†, Lawrence Weintraub†, Richard Dickinson†, Ronald Bloom†, Grant Karamyan†, Anneliese Lilje†*

* Jet Propulsion Laboratory, California Institute of Technology, 4800 Oak Grove Drive, Pasadena, CA 91109

Phone: 818 354-3322, Email: scott.hensley@jpl.nasa.gov

†The Aerospace Corporation, 2310 E. El Segundo Blvd., El Segundo, CA 90245

ABSTRACT

Mapping the Moon's topography using Earth based radar interferometric measurements by the Goldstone Solar System Radar (GSSR) has been done several times since the mid 1990s. In 2008 we reported at this conference the generation of lunar topographic maps having approximately 4 m height accuracy at a horizontal posting of 40 m. Since then GSSR radar has been improved to allow 40 MHz bandwidth imaging and consequently obtained images and interferograms with a resolution of about 4 m in range by 5 m in azimuth. The long synthetic aperture times of approximately 90 minutes in duration necessitated a migration from range/Doppler image formation techniques to spotlight mode processing and autofocusing methods. The improved resolution imagery should permit the generation of topographic maps with a factor of two better spatial resolution with about same height accuracy. Coupled the with the recent availability of new lidar topography maps of the lunar surface made by orbiting satellites of Japan and the United States the geodetic control of the radar generated maps products can be improved dramatically. This paper will discuss the hardware and software improvements made to the GSSR and present some of the new high resolution products.

1. INTRODUCTION

Earth-based radar observations of the Moon have played a major role in interpreting the geology of the Moon and understanding the composition of the lunar regolith. The GSSR radar has played a major role in providing data used to interpret and understand the composition and geological history of the lunar surface. One of the most valuable pieces of information for understanding both composition and geologic history as well as being of central importance to either robotic manned exploration of the moon are accurate topographic maps of its surface. Figures 1a-1c show images of the radar magnitude, elevation and elevation errors respectively generated from the GSSR radar from data collected on September 13 and December 5 of 2006, [4]. The elevation data generated in 2008 had a posting of 40 m with an actual spatial resolution closer to 60-70 m meters resulting from low pass filtering of the interferometric phase data prior to map formation. The average elevation accuracy as determined from the correlation data was 12.8 m with a standard deviation of 14.3 m for all points in the map including points mapped very close to the null in the mainlobe of the transmit antenna DSS-14 where elevation errors grew to around 50 m. For points in the central portion of the mainlobe elevation accuracy was in the 3-5 m range far exceeding the accuracy of previously generated maps.

At the time these maps were initially generated the best available geodetic control was the United Lunar Control Network 2005 (ULCN 2005) which is based primarily on Clementine data. Estimated elevation errors for points in that data set varied from several hundred to several thousand meters which is considerably larger than the 5 m accuracy of the GSSR data. Since the time we initially generated the GSSR based lunar topographic maps, three spacecraft from India, Japan and the United States were sent to the moon with the capability of making elevation measurements. The Indian spacecraft, Chandrayaan, is generating topographic data using photogrammetric stereo techniques, whereas the the Japanese spacecraft, Kaguya, and the United States spacecraft, Lunar Reconnaissance Orbiter (LRO), have lidars for making topographic measurements. These systems are all capable of making elevation measurements with accuracy far exceeding the data in the UNLC 2005 database and thus are far more suitable for geodetic control. Kaguya data for example has a reported accuracy of 10 m, [1] which we have employed for geodetic control of the data shown in Figure 1. A comparison of the Kaguya and GSSR elevation data near the pole were consistent with a lidar elevation noise level of 10 m and a radar elevation noise level of 5 m.

Even with the advent of the Kaguya and soon to be released LRO topographic data sets there is still value from having the capability to generate topographic maps using the GSSR radar. The lidar based topographic maps from LRO and Kaguya have excellent height accuracy, however they will only be able to generate topographic maps with 20 m postings within a small region (about a degree) about the pole and will have around 1 km postings near the equator. The recently improved GSSR radar, which now has the capability to transmit 40 MHz bandwidth linear frequency modulated (LFM) or chirp waveforms, can generate topographic maps with 20 m postings (4 m imagery) anywhere on the near side of the Moon with about 5 m elevation height accuracy depending on the number of images mosaicked to make the

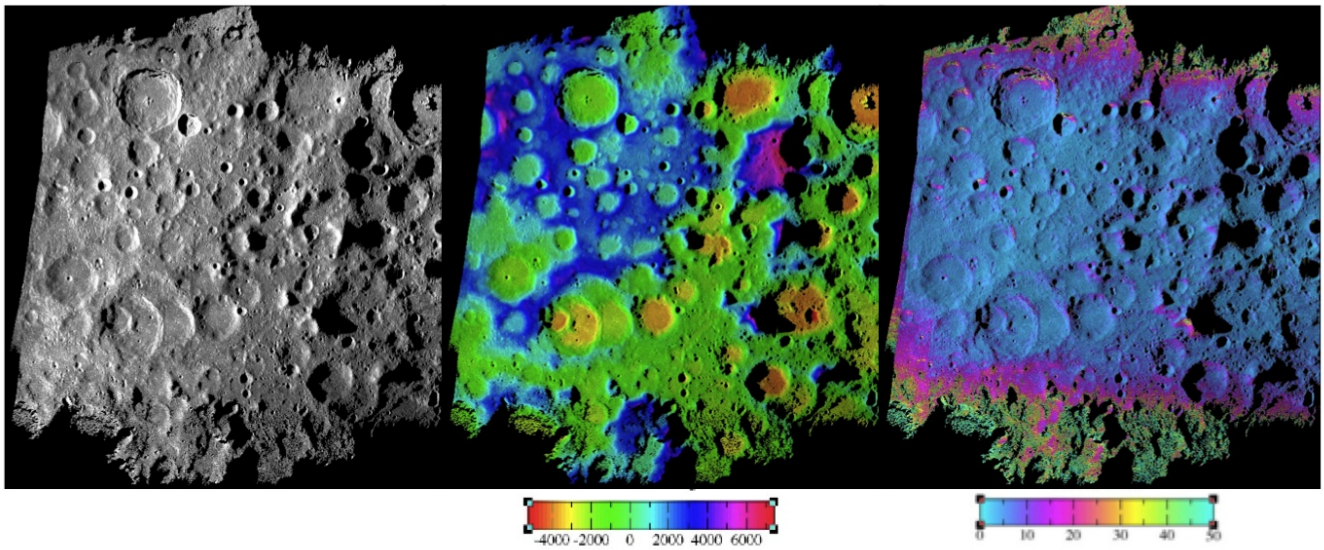

Fig. 1. *The left most image is the GSSR radar magnitude image, the middle image is the elevation map and the right most image is the elevation error map.*

final map product. This paper discusses changes made to the GSSR hardware and processing systems to make this possible.

2. HARDWARE UPGRADES TO THE GSSR SYSTEM

The GSSR radar system consists of a series of transmitting and receiving antennas located near the Goldstone Lake Bed in the Mojave Desert of California. The GSSR interferometric observations of the Moon involve transmitting an X-band (3 cm wavelength) signal on the 70 m antenna, DSS 14, and receiving on two 34 m antennas (DSS 13 and 25) that have an interferometric baseline of 13 km. Figure 5 shows the relative positions of the transmitting and receiving antennas comprising the GSSR interferometric radar observation system. Previous interferometric data collected by the GSSR system employed a continuous transmitting Pseudo-Random Noise (PN) phase-coded waveform of length 131070. The time interval between each 180° phase shift, called a chip, is 0.125 μs which results in a total transmitted code duration of 16.4 m̃s. This is greater than the lunar range depth (11.6 ms), thereby allowing polar imagery to be collected without range ambiguities. This chip length gives a range resolution of 18.75 m. Several waveform options were considered for increasing the range resolution of the GSSR system with special care devoted to insuring the out of band emissions would meet NTIA requirements and that were compatible with the 500 kW klystron used for the transmitted signal. Table I provides an overview of the GSSR radar parameters after modification. A brief overview of the modifications to the GSSR system are presented below.

2.1 Transmitter

The signal path for the transmitter is shown in Figure 3. The in-phase and quadrature-phase components of the radar waveform are generated using a Gage CompuGen 4300 waveform generator. The singled ended output of each channel is

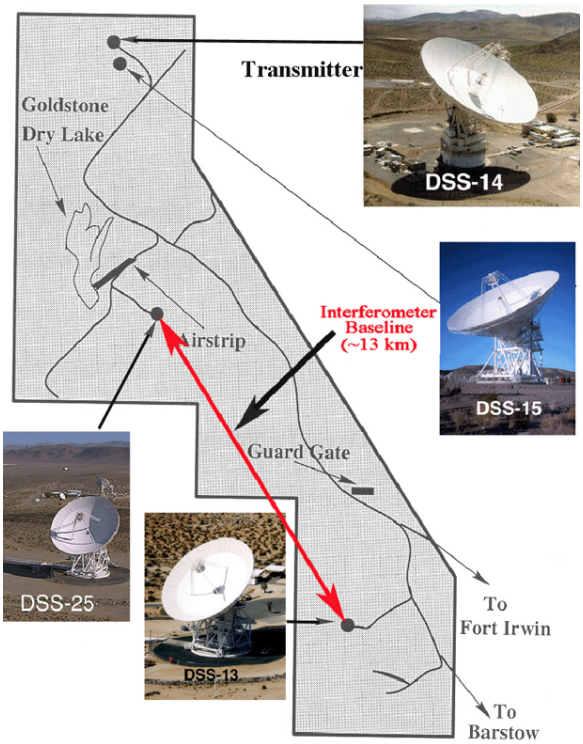

Fig. 2. *The GSSR interferometer consists of a 70 m transmit antenna and two 34 m receive antennas separated by 13 km.*

independently filtered with a cascade of two 39 MHz low-pass filters. The filter outputs are fed into a pair of Analog Devices differential amplifier evaluation boards generating differential signals for each channel that are fed into an Analog devices quadrature modulator evaluation board. The quadrature modulator mixes the in-phase and quadraturephase inputs with the 560 MHz intermediate-frequency (IF) carrier generated from an Agilent E8663B frequency synthesizer. The modulated IF

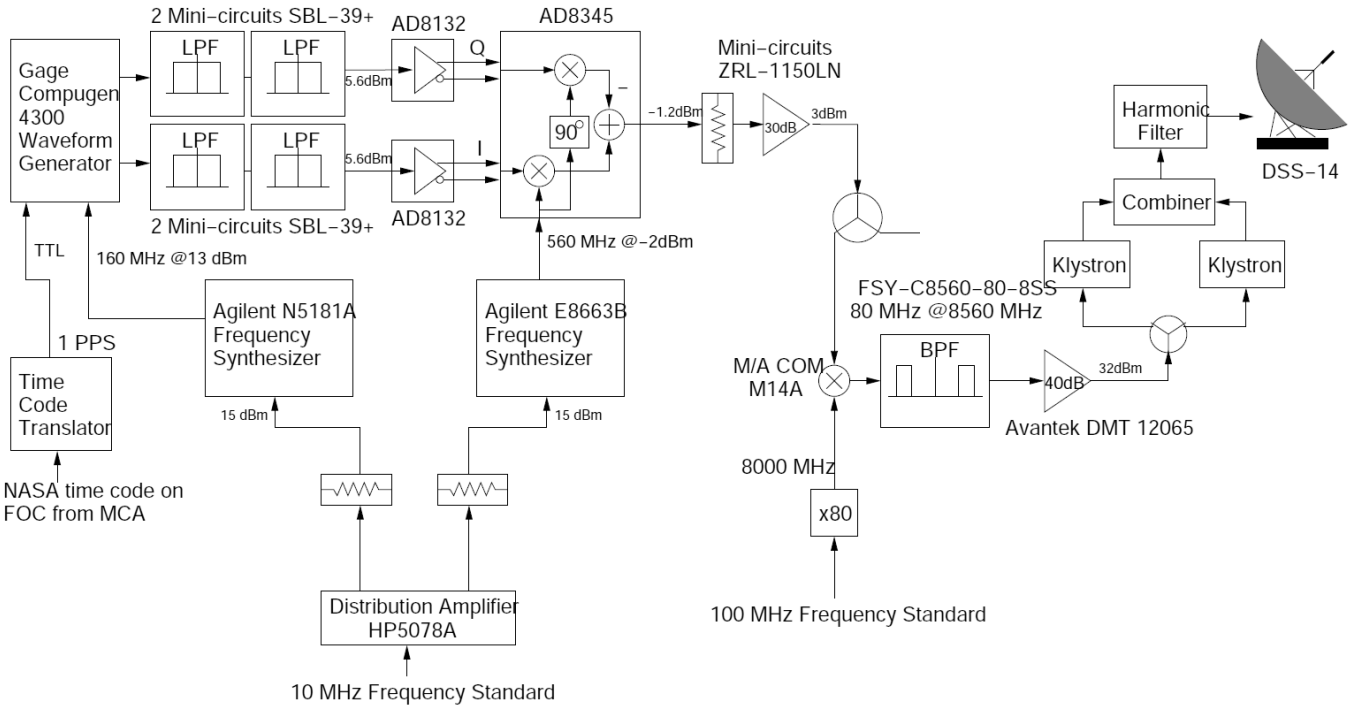

Fig. 3. *Transmit signal path at DSS-14*

TABLE I
GSSR SYSTEM PARAMETERS

Parameter	Value
Radar band	X-band
Pulse bandwidth	40 MHz
Pulse modulation	Linear FM chirp
Range resolution	4 m
Standoff range	370,000 km
Pulse duration	12.5 or 20 msec
Pulse repetition frequency	50 or 80 Hz
Synthetic aperture time	90 min.
Synthetic aperture length	2,300 km
Cross-range resolution	5 m
Area coverage	430,000 km^2

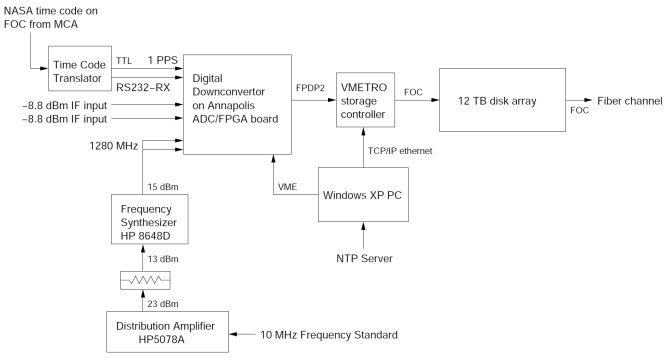

Fig. 4. *Data acquisition system*

carrier is then amplified using a low-noise amplifier and mixed with a 8000 MHz carrier generated from a 80× frequency multiplication of the 100 MHz station frequency standard. The resulting X-band modulated carrier is filtered using an 80 MHz bandpass filter centered at 8560 MHz and is fed into a 4 W amplifier followed by a splitter and pair of 250 kW Klystron amplifiers whose outputs are combined and fed to the antenna waveguide to generate near 500 kW of continuous modulated power.

2.2 Receiver

The received signals from DSS-13 and DSS-25 are each downconverted, sampled, and stored for interferometric processing. Each station has m antenna followed by a low noise amplifier. The RF signal is then down-converted to a 460 MHz IF that is routed to DSS-14 where IF sampling and digital down-conversion occurs. At DSS-13, the IF signal passes through an electro-optical converter connected via optical fiber to an optical-electro converter at DSS-14. At DSS-25, the IF signal is routed to DSS-14 electrically using the host-country port at SPC-10. The pair of IF signals, now at DSS-14, are passed through a distribution amplifier/attenuator and separately routed to an Annapolis Micro Systems Wildstar II VME ACE processing and ADC board which acts as a pair of digital downconverters producing samples of the in-phase and quadrature phase baseband signals for each station. The baseband sampled data is stored, using a VMetro VME disk controllers that manage the storage into a 12 TB disk raid array as shown in Figure 4.

3. DATA ACQUISITIONS AND DATA PROCESSING

After testing the hardware modifications to the GSSR hardware, three acquisitions using the increased 40 MHz

TABLE II
GSSR 40 MHz DATA COLLECTIONS

Acquisition Date	Duration
May 22, 2009	180 min (2 90 min apertures)
July 15, 2009	360 min (4 90 min apertures)
November 1, 2009	360 min (4 90 min apertures)

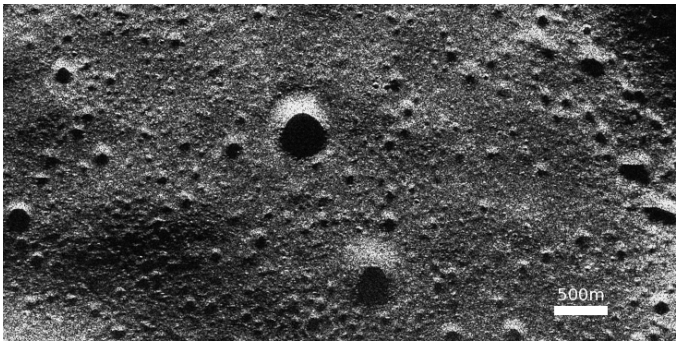

Fig. 5. *Imagery processed to approximately 9 m from the 40 MHz GSSR data.*

bandwidth LFM waveform were acquired of the south polar region of the Moon as shown in Table II.

Processing of the lunar data begins by segmenting the 180 min or 360 min collections into groups of pulses commensurate with the amount of integration time needed to process the data to the desired resolution in the cross-range direction, *i.e.* commensurate with the required synthetic aperture length. Each data segment or look is processed into imagery and topographic maps using the process described in the following and then in a mosaicking step combined into the final image and topographic map products. Since the noise in uncorrelated between looks, the height error is reduced by the square root of the number of looks. To achieve the desired 5 m image resolution requires an integration time of approximately 90 minutes and hence the data will be segmented into 2-4 independent looks. The finer resolution imagery coupled with the large image size of 400 km by 600 km has resulted in a number of modifications to the processing pipeline compared to our earlier effort discussed previously. The major elements are discussed below.

3.1 Spotlight Mode SAR Image Formation

Image formation begins with the signal data collected from the two GSSR receive antennas for each look being processed to single look complex (SLC) images using a convolutional matched filter to compress the chirp coded waveform in the range direction and a spotlight mode processing algorithm for azimuth or cross-range compression. The finer resolution of the modified GSR system and the accompanying migration through resolution cells during a synthetic aperture called for spotlight, rather than delay-Doppler, imaging techniques. A new pre-processing system supports fast-time Doppler removal and motion compensation to a point. Two spotlight imaging techniques which compensate for phase errors due to i) out of focus-plane motion of the radar and ii) local topography, have been implemented and tested. One is based on the polar format algorithm followed by a unique autofocus technique, the other is a full bistatic time-domain backprojection technique. Figure 5 shows an 9 m resolution image of a portion of the south pole GSSR processed using the spotlight mode techniques, Using an appropriately chosen lunar elevation reference good focusing is obtained without autofocus, however, for the longer synthetic aperture times required for 5 m processing topographic effects cause defocusing which is compensated by autofocus. Products enabled by this new system include topographic mapping through radar interferometry, and change detection techniques (amplitude and coherent change) for geolocation of the NASA LCROSS mission impact site and potentially for future studies of small meteor impacts on the lunar surface. Details of the processing enhancements are discussed in the companion paper [3].

3.2 Interferogram Formation and Filtering

The high resolution and long synthetic aperture times preclude processing the entire scene at one time, so the image is subdivided into approximately 100 km by 100 km overlapping images referred to as patches. The amount of overlap between patches is approximately 10 km to allow enough data for relative elevation adjustments in the mosaicking process. Subsequent to the image formation process is the interferogram generation process. Since autofocus techniques are required to obtain full resolution imagery extreme care must be taken to avoid phase discontinuities in the interferogram. To minimize phase discontinuities, that will translate into height discontinuities, the following procedure has been adapted. First, the imagery from each channel is focused using the spatially variant autofocus from one of the channels in order to optimize the match quality used to register the two images. The autofocus cell size is a fraction of the patch size (about 1/20) and the results of overlapping autofocus cells are feathered to avoid phase discontinuities. Then using the offset measurements the second unautofocused image is resampled to the first unautofocused image and the spatially variant autofocus procedure in run again on the now co-registered imagery. Finally, the same autofocus correction generated from a combination of the autofocus results from the two channels is applied to both channels. Figure 6 shows an interferogram generated from 4 m resolution GSSR radar data.

A measure of the quality of the interferogram is the interferometric correlation, γ, which is a measure of the similarity of the signals received on the two channels. The amount of phase noise in the interferogram, σ_ϕ, is related to the correlation by

$$\sigma_\phi = \frac{1}{\sqrt{2N_L}}\sqrt{\frac{1-\gamma^2}{\gamma^2}} \tag{1}$$

where N_L is the number of pixels averaged together in forming the interferogram. One of the nice features of interferometric mapping systems is the ability to estimate the elevation accuracy for each pixel in the DEM using the interferometric

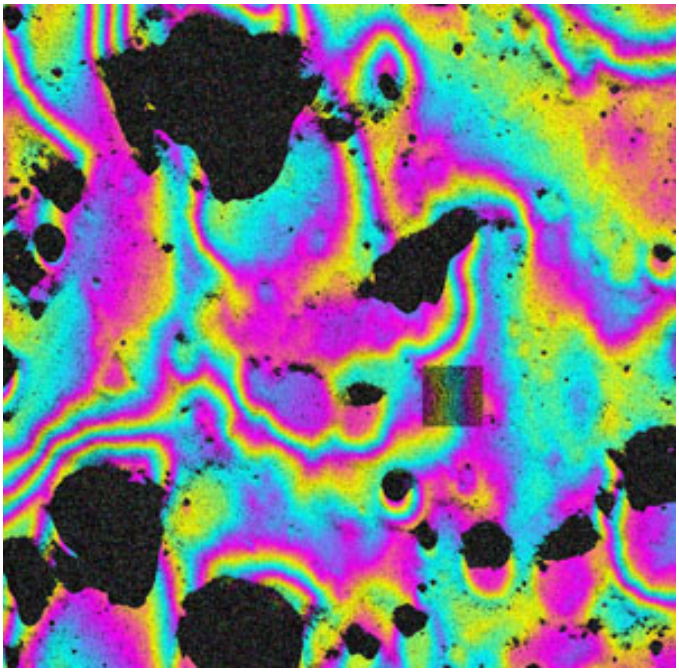

Fig. 6. *Interferogram formed from 4 m GSSR imagery of the south polar region of the Moon. Sixteen looks, 4 in range and azimuth, were used to form this interferogram. An autofocus cell size is illustrated in the central portion of the interferogram.*

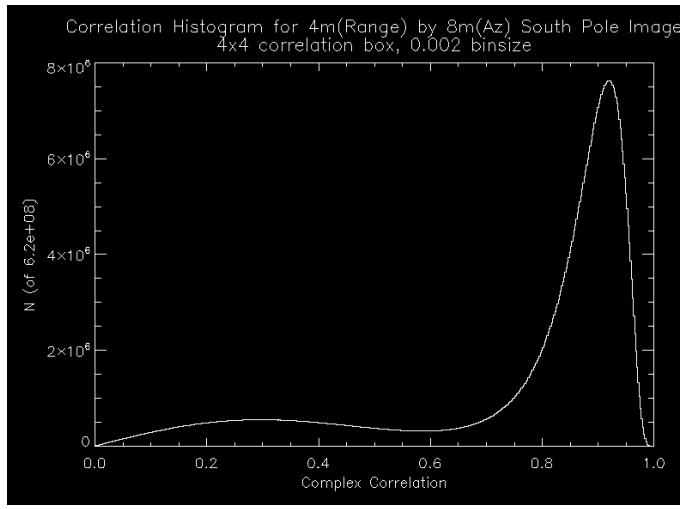

Fig. 7. *Histogram of the interferometric correlation obtained from 4 m GSSR imagery. The high correlation, mean of 0.92, shows that hardware and processing subsystems are working well.*

correlation. Topographic map accuracy is a function of the sensitivity of the phase to height and from Equation 1 an estimate of the height accuracy, σ_h, is given by

$$\sigma_h = \frac{\partial h}{\partial \phi}\sigma_\phi = \frac{1}{\sqrt{2N_L}}\sqrt{\frac{1-\gamma^2}{\gamma^2}}\frac{1}{2\pi}h_a \tag{2}$$

where

$$\frac{\partial \phi}{\partial h} = \frac{2\pi p}{\lambda}\frac{1}{\langle \hat{\ell}, \hat{n}\rangle}\left\langle \vec{b}, \frac{1}{\rho}\left(-\hat{\ell} + \frac{\hat{g}}{\langle \hat{\ell}, \hat{g}\rangle}\right)\right\rangle \tag{3}$$

$$\hat{g} = \frac{\hat{\ell} - \langle \hat{\ell}, \hat{n}\rangle \hat{n}}{|\hat{\ell} - \langle \hat{\ell}, \hat{n}\rangle \hat{n}|} \tag{4}$$

$$h_a = \left(\frac{\partial \phi}{\partial h}\frac{1}{2\pi}\right)^{-1} \tag{5}$$

where λ is the radar wavelength, ρ is the range, $\vec{b}$ is the interferometric baseline, i.e., the vector difference of the two antenna locations in the interferometric pair, $\hat{\ell}$ is the unit look vector pointing from the reference antenna position to the scatterer and p=1,2 depending on whether the interferometer is operated in the single antenna transmit or ping-pong configuration (transmitting alternately on both antennas).and $\hat{n}$ is the local normal to the lunar surface.

Figure 7 shows a histogram of the correlation obtained from the 4 m GSSR interferometric data. The mean of 0.92 translates into a phase noise of 0.075 radians for 16 looks that in turn gives a elevation error of about 12 m for a 20 m pixels using Equation 3. From the 3 GSSR collections described previously we expect to have 10 independent images that we can combine that will reduce the height error per pixel by $\sqrt{10}$ to about 4 m similar to our previous map but with 3 times better spatial resolution.

3.3 DEM Generation

In order to determine the three dimensional position of a point, we need three observations. A single SAR image provides two observations consisting of the range and Doppler to a pixel. The third observation is obtained from the phase of an interferogram that is formed by multiplying the complex value of a pixel in one image by the complex conjugate of the corresponding pixel in the second image of the interferometric pair. The range, ρ, Doppler, f, and interferometric phase, ϕ, measurements are given by

$$\rho = |\vec{T} - \vec{P}| \tag{6}$$

$$f = \frac{2\langle \vec{v}, \hat{\ell}\rangle}{\lambda} \tag{7}$$

$$\phi = \frac{2\pi p}{\lambda}\rho\left(\sqrt{1 - \frac{2\langle \hat{\ell}, \vec{b}\rangle}{\rho} + \left(\frac{b}{\rho}\right)^2} - 1\right) \tag{8}$$

where $\vec{T}$ is the scatterer position vector, $\vec{P}$ is the position vector of the reference antenna in the interferometric pair and $\vec{v}$ is the velocity vector, ϕ is the phase of the complex value in the interferogram that contains the topographic height information. However, the interferometric phase is only measured modulo 2π, which represents only a fraction of the unambiguous differential range distance between the two antennas. Since the phase corresponding to the differential range distance can be many multiples of 2π, a two dimensional phase unwrapping procedure is applied to retrieve an unambiguous phase measurement. We use a modified version of the residue based unwrapping algorithm that was employed by the Shuttle Radar

Topography Mission (SRTM) to map the Earth's elevation in 2001 [2].

The three dimensional scatterer location, $\vec{T}$, is solved for via

$$\begin{aligned}\vec{T} &= \vec{P} + \rho\left(\frac{\lambda f}{2v}\hat{v}\right. \\ &+ \frac{\frac{b^2}{2\rho} - \frac{\lambda\phi}{2\pi p}\left(1+\frac{\lambda\phi}{4\pi p\rho}\right) - \langle\vec{b},\hat{v}\rangle\frac{\lambda\rho f}{2v}}{b\sqrt{1-\langle\hat{b},\hat{v}\rangle^2}}\frac{(\vec{v}\times\vec{b})\times\vec{v}}{|(\vec{v}\times\vec{b})\times\vec{v})|} \\ &\pm \left.\sqrt{1-\langle\hat{\ell},\hat{v}\rangle^2-\langle\vec{\ell},\hat{n}\rangle^2}\frac{\vec{v}\times\vec{b}}{|\vec{v}\times\vec{b}|}\right) \qquad (9)\end{aligned}$$

where $\hat{n} = \frac{(\vec{v}\times\vec{b})\times\vec{v}}{|(\vec{v}\times\vec{b})\times\vec{v})|}$. Scatterer location is a function of the baseline, velocity and platform position vectors and the range, phase and Doppler observables. Very precise knowledge of each of these quantities is required to achieve an accurate height map. Height reconstruction is done in a Moon centered Moon fixed coordinate system then converted into the desired polar stereographic map projection.

3.4 Mosaicking

The height maps from each individual patches and looks are combined in a mosaicking process that weights the data by the height error estimate described above. Let $\{(h_i, \sigma_i, f_i), 1 \le i \le N_L\}$ be a set of triples consisting of a height measurement, h_i, height error estimate, σ_i, given by Equation 2 and feathering weights, f_i. Feathering weights at a point p, $f_i(p)$, are computed based on the minimum distance to a boundary point and a user specified feathering distance, F_l, which was set to 50 pixels, by

$$f_i(p) = \min_{x\in\mathcal{B}_i}\frac{\min(d(p,x),F_l)}{F_l} \qquad (10)$$

where $\mathcal{B}_i$ is the set of boundary points in in the ith look, *i.e.* points for which no elevation measurement is available and $d(p,x)$ is the euclidean distance in pixels from p to x. Combining the heights to obtain a minimal variance height estimate uses the weighted sum of the individual height estimates where the weight is inversely proportional to the square of the estimated height error and proportional to any feathering weight that is applied. Note the following formulation assumes all height errors are uncorrelated. The final combined height, h_f, is given by

$$h_f = \sum_{i=1}^{N}\frac{\left(\prod_{i\neq j}^{N}\sigma_j^2\right)f_i}{\sum_{k=1}^{N}\left(\prod_{j\neq k}^{N}\sigma_j^2\right)f_k}h_i \qquad (11)$$

The height error, σ_{h_f}, of the combined height estimate is given by

$$\sigma_{h_f} = \left(\prod_{j=1}^{N}\sigma_j^2\right)\left(\sum_{i=1}^{N}\frac{f_i^2}{\sigma_i^2\left(\sum_{k=1}^{N}\left(\prod_{j\neq k}^{N}\sigma_j^2\right)f_k\right)^2}\right)^{\frac{1}{2}} \qquad (12)$$

4. CONCLUSIONS AND FUTURE WORK

Interferometric radar data of the Moon collected by the upgraded GSSR system in 2009 are being used to generate the most accurate topographic maps of its south polar region. The final map products are expected to have a planimetric resolution of 20 m and a relative vertical accuracy (1 σ) of 3-5 m. These products can be used to support scientific investigations including the search for ice deposits in permanently shadowed craters on the lunar surface and to aid in mission planning and exploration for future lunar missions. These data will also be used to support several scientific investigations concerning the geologic history of the moon and the formation of lunar geologic features. The absolute accuracy of these topographic maps will be significantly enhanced by making synergistic use of the lidar topographic data that is being collected by satellites of Japan and the United States.

ACKNOWLEDGMENT

This research was conducted at the Jet Propulsion Laboratory, California Institute of Technology, under contract with the National Aeronautics and Space Administration. Reference herein to any specific commercial product, process, or service by trade name, trademark, manufacturer, or otherwise, does not constitute or imply its endorsement by the United States Government or the Jet Propulsion Laboratory, California Institute of Technology.

The authors would like to thank the Aerospace Corporation for supporting the work through the Independent Research and Development Program.

References

[1] H. Araki, S. Tazawa, H. Noda, Y. Ishihara, S. Goossens, S. Sasaki, N. Kawano, I. Kamiya, H. Otake, J. Oberst, and D. Shum. Lunar global shape and polar topgraphy deiuved from kagyua-lalt laser altimetry. *Science*, 323:897–900, 2009.

[2] Tom Farr, Paul Rosen, Edward Caro, Robert Crippen, Riley Duren, Scott Hensley, Michael Kobrick, Mimi Paller, Ernesto Rodriguez, Ladislav Roth, David Seal, Scott Shaffer, Joanne Shimada, Jeffrey Umland, Marian Werner, Michael Oskin, Douglas Burbank, and Douglas Alsdorf. The shuttle radar topography mission. *Rev. Geophys*, 45, 2004.

[3] L. Harke, L.Weintraub, Sang-Ho Yun, Richard Dickinson, Eric Gurrola, Scott Hensley, and Nicholas Marechal. Spotlight-mode synthetic aperture radar processing for high-resolution lunar mapping. In *Proceedings of the Radarcon 2010, Washington DC, USA*. IEEE Press, May 2010.

[4] Scott Hensley, Eric Gurrola, Paul Rosen, Martin Slade, Joseph Jao, Mike Kobrick, Barbara Wilson, Curtis Chen, and Raymond Jurgens. An improve map offset the lunar south pole with earth based radar interferometry. In *Proceedings of Radrcon 2008, Rome Italy*. IEEE Press, May 2008.